



A Hybrid Switching Technique for Single-Phase AC-Module PV System to Reduce Power Losses and Minimize THD

H. Toodeji^{*(C.A.)}

Abstract: This paper proposes a hybrid switching technique for a domestic PV system with AC-module architecture. In this PV system, independent control of PV modules, which are directly connected to DC terminals of a single-phase cascaded multilevel inverter, makes module-level MPPT possible to extract maximum available solar energy, especially in partial shading conditions. As one of the main contributions, the proposed hybrid method employs a fundamental-based switching technique to decrease power losses, which directly affect the efficiency of solar energy conversion. In addition, fast dynamic response of the introduced hybrid technique lets the PV system to harvest more power in partial shading conditions. Producing a waveform with minimized THD in steady-state conditions is another advantage of the proposed switching technique. In this paper, the advantages of the proposed hybrid method are verified by the simulation of a test PV system with both conventional SPWM and proposed switching techniques in MATLAB/Simulink under various partial shading conditions.

Keywords: Cascaded Multilevel Inverter, Fundamental Frequency Switching Technique, Single-Phase PV System, Switching Losses, THD Minimization.

1 Introduction

NOWADAYS, small-scale PV systems are increasingly installed all around the world from isolated rural spaces to residential areas [1, 2]. To harvest the highest possible solar energy from these PV systems, different maximum power point tracking (MPPT) methods are introduced. Conventional MPPT methods can correctly find the optimal operating point when all PV modules experience the same conditions [3]. However, they are unable to track the globally optimal point in mismatched operating conditions in which multiple local optima will be arisen [4]. As a result of the suboptimal operation of some PV modules, the total harvested power is significantly affected [5]. In addition, the creation of hot spots in the suboptimal PV modules results in their fast deterioration

[6].

The mismatch in operating conditions is mainly caused by nonuniform illumination in which some PV modules experience different solar radiation, partially or totally [7]. For instance, building-integrated photovoltaic (BIPV) systems endure such conditions, because PV modules may be installed on a curved surface [8]. Besides, surrounding obstacles in urban environments or shading of one PV module to another in compact installations often lead to partial shading conditions. In addition, there are environmental phenomena such as bird droppings and moving clouds, as fixed and moving shadings, respectively, that block/decrease received sunlight by some PV cells for a while [9].

To extract maximum power and prevent damage to PV modules in partial shading conditions, various methods have been proposed. These methods can be categorized in the following four groups: utilizing developed MPPT techniques [10], changing the configuration of PV arrays [11], using appropriate architectures [12-14], and employing novel converter topologies [15]. In AC-module architecture, each PV module is connected to its own microinverter, so module-level MPPT can be carried out to harvest more

Iranian Journal of Electrical and Electronic Engineering, 2020.

Paper first received 27 September 2019, revised 14 November 2019, and accepted 16 November 2019.

* The author is with the Electrical Engineering Department, Yazd University, Yazd, Iran.

E-mail: toodeji@yazd.ac.ir

Corresponding Author: H. Toodeji.

power in partial shading conditions. It is worth mentioning that this microinverter can be the stages of a cascaded multilevel inverter.

In some PV systems with AC-module architecture, a DC-DC converter, also known as power optimizer, is employed beside or merged in each microinverter to perform module-level MPPT [16, 17]. It is worth mentioning that more than 55% of domestic PV systems in the USA have utilized various combinations of local power optimizer and microinverter, known as module-level power electronics (MLPE), as one of the fastest growing markets in the solar industry, in 2014 [18]. However, some studies have introduced various module-level MPPT structure with no need for local power optimizers [12]. Elimination of local power optimizers reduces the size, cost and control complexity of PV systems and also increases the reliability as well as the efficiency of the PV system.

In the present paper, a hybrid switching technique is proposed for a single-phase PV system with the cascaded multilevel inverter. In this AC-module architecture, PV modules are directly connected to the DC terminals of multilevel inverter without any DC optimizer. One of the main contributions of the hybrid switching technique is power losses reduction that improves the efficiency of the solar energy conversion system. This purpose is obtained by employing a fundamental frequency-based switching technique, however slower dynamic response of such techniques may inversely affect total harvested power in comparison with conventional SPWM. To deal with this concern, both SPWM and fundamental frequency techniques are combined in the hybrid technique to improve the dynamic response. As another contribution, the THD value of the produced waveform in steady-state conditions is minimized to meet the limits of available harmonic standards.

This paper is organized as follows; the configuration of the single-phase AC-module PV system is presented in Section 2 and then, the proposed hybrid switching technique for this PV system is overviewed in the next section. Section 4 is dedicated to explaining the modified decoupled current controller and a detailed description of the proposed two-step hybrid switching technique can be found in Section 5. Section 6 is devoted to the simulation of a test PV system with both conventional SPWM and proposed hybrid switching techniques in MATLAB/Simulink under various partial shading conditions. Comparing the obtained results can verify the advantages of the hybrid switching technique over conventional SPWM.

2 Configuration of Single-Phase AC-Module PV System

The configuration of a single-phase PV system with the AC-module structure is presented in Fig. 1. It is seen that each PV module is directly connected to a specific

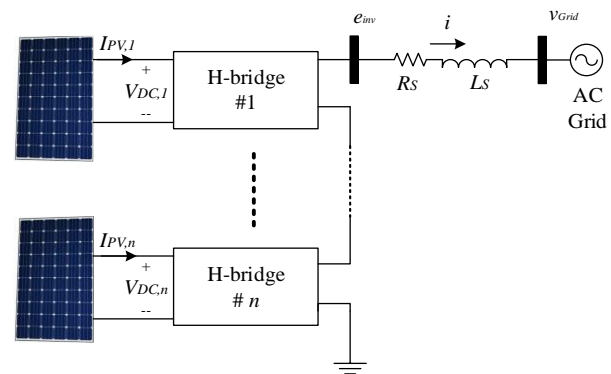


Fig. 1 Single-phase AC-module PV system.

H-bridge of the cascaded multilevel inverter. Moreover, the multilevel inverter is connected to the single-phase AC grid through a first-order filter decreasing the harmonic content of injected current. In spite of the fact that R_S and L_S represent the resistance and inductance of harmonic filter, respectively, Thevenin's impedance of the AC grid at point of common coupling (PCC) are also considered in this impedance. It is noteworthy that other higher-order harmonic filters, like LC and LCL, can also be utilized instead of the present first-order filter, considering the limits of a specific harmonic standard.

3 An Overview of the Proposed Hybrid Switching Technique

In this section, the proposed two-step hybrid switching technique for the presented AC-module PV system is overviewed. As expected, the switching technique should consider both steady-state and transient conditions. The main concern of steady-state condition is power losses reduction as well as THD minimization, so a fundamental frequency-based switching technique is employed instead of the conventional SPWM. In addition, the proposed switching technique should also be able to utilize a simple MPPT method, such as standard perturb & observe (P&O), to perform module-level MPPT in the PV system with AC-module structure.

In the standard P&O method, which is described by the discrete-time dynamic model in (1) and presented in Fig. 2, the variation of PV voltage (ΔV_{PV}) and power (ΔP_{PV}) are employed to produce controlled perturbation command.

$$x(k+1) = x(k) + [V_{pv}(k) - V_{pv}(k-1)] \cdot \text{sgn}(P_{pv}(k) - P_{pv}(k-1)) \quad (1)$$

where sgn represents the signum function and $x(k)$ an internal perturbation variable to generate the MPPT control signal [19].

Obviously, a fundamental frequency-based technique needs more time to perform this MPPT method, since it cannot quickly change PV voltages. Therefore, employing this switching technique for both steady-state and transient conditions can inversely affect the

dynamic response. Moreover, ambient conditions may also be varied during such a time-consuming procedure for some PV modules due to a transient shadow such as fast-moving clouds on a windy day.

To improve the dynamic response, the conventional SPWM technique is employed in step 1 having fast MPPT. However, additional power losses due to utilizing the SPWM technique can be neglected, since partial shading conditions do not happen frequently and also new MPPs can be quickly found. Moreover, fast MPPT decreases the suboptimal operation interval of partially shaded PV modules, so the harvested power as well as the efficiency of the PV system increase.

Due to the inherent oscillatory response of the standard P&O method [19], power variation (ΔP) smaller than ϵ_p is considered as finishing of MPPT procedure in step 1, as seen in Fig. 3. Upon finding the optimal operating point, step 2 starts and the switching technique is returned to the fundamental frequency-based technique to reduce the power losses. It should be noted that the required switching angles to regulate modules' voltages at their recently found optimal values are quickly calculated in substep 1 before changing the switching technique. These switching angles may result in waveforms with high THD amounts since there is no control on THD value. Finding optimal switching angles for THD minimization as well as DC voltage regulation in substep 2 is a time-consuming procedure. On the other hand, continue to operation in SPWM until the end of this optimization procedure increases the power losses. Thus, the proposed switching technique employs SPWM only for finding MPP and then immediately returns to the fundamental frequency-based technique with suboptimal switching angles until the calculation of optimal angles I substep 2.

In addition to finalizing step 1, more attention to Fig. 3 clears that modulation index changes (ΔM) bigger than ϵ_M can also activate step 2. Such change may happen solely due to variations of reactive power

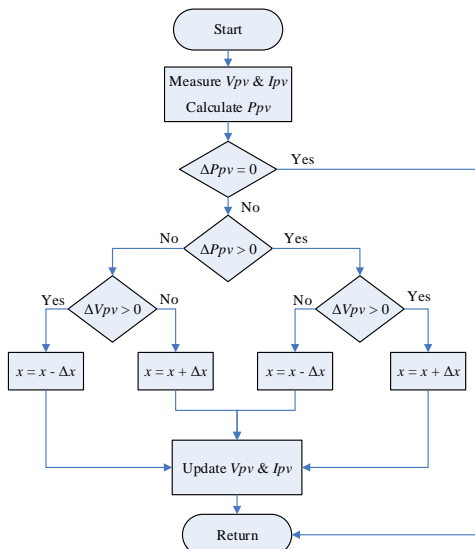


Fig. 2 Flowchart of the standard P&O method [19].

reference in the modified decoupled current controller. Therefore, those conditions with ΔM bigger than ϵ_M and ΔP smaller than ϵ_p are directly conducted to step 2 preventing unnecessary activation of step 1.

4 Modified Decoupled Current Control

The lowest level of the hierarchical controller for the PV system, which generates gate signals for multilevel inverter, is commanded by a modified decoupled current controller as its upper control level. In the well-known structure of the decoupled current controller, which is

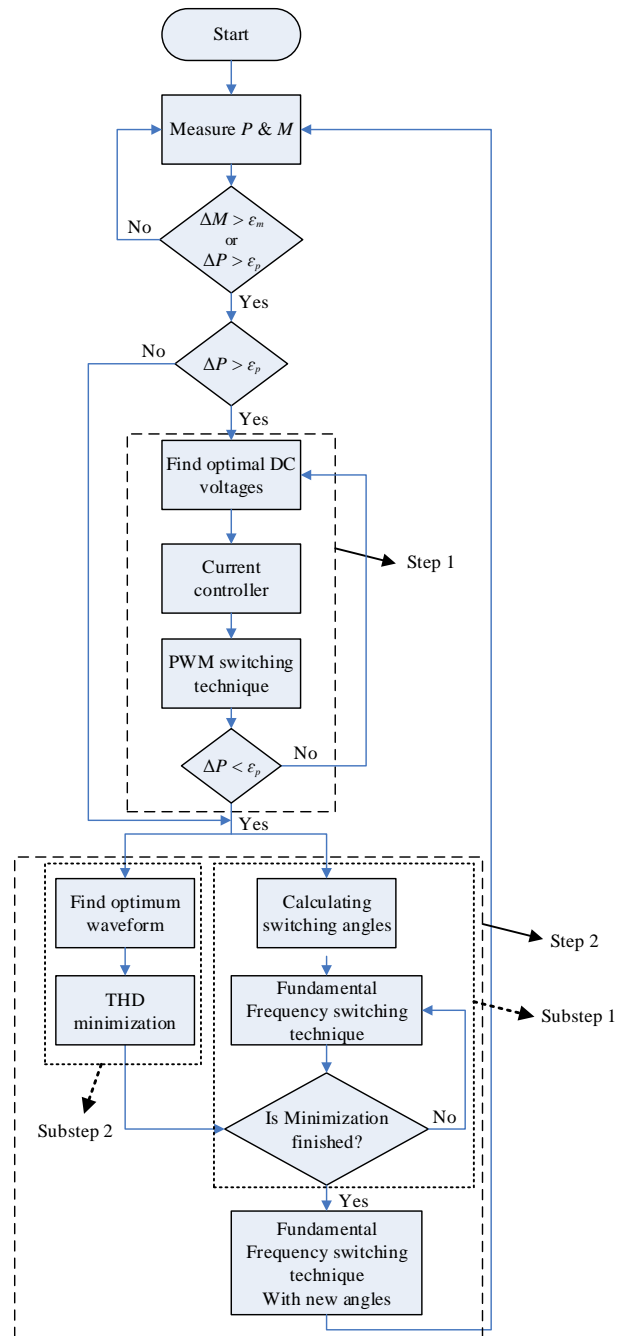


Fig. 3 Flowchart of the proposed two-step hybrid switching technique.

commonly used in three-phase systems, derived equations are transformed from stationary abc to quadratic rotary dq frame. This transformation can be applied to those systems with at least two independent phases, so dq model of the present single-phase circuit cannot be directly obtained. To solve this problem, an imaginary orthogonal circuit, which is constructed at the basis of the real circuit, can be assumed as the second independent circuit. The components of this imaginary circuit are similar to that of the real circuit, but with 90° phase-shifted state variables. One may consider a specific delay in the real circuit to achieve the desired phase-shift, but this delay inversely affects dynamic response [20]. Differentiation, as an alternative solution, can also result in the desired phase-shift with no impact on dynamic performance [21]. For instance, $x_I(t)$ in (2) is a state variable of an imaginary circuit, which is obtained by differentiation of $x_R(t)$, as a state variable of real single-phase circuit:

$$\begin{cases} x_R(t) = A_R \sin(\omega t + \varphi) \\ x_I(t) = \frac{d x_R(t)}{dt} = A_I \cos(\omega t + \varphi) \\ A_I = \omega A_R \end{cases} \quad (2)$$

where A_R and A_I are the amplitude of real and imaginary state variables, respectively, ω is the fundamental angular frequency in rad/sec and φ is the initial phase angle in rad. Also, the amplitude of the imaginary state variable is multiplied by $1/\omega$ after differentiation.

Now, the given transformation matrix T in (3) can be utilized to determine d - and q -axis components of single-phase state variables in dq coordinates, which are respectively shown by x_d and x_q in (3).

$$\begin{bmatrix} x_d \\ x_q \end{bmatrix} = T \cdot \begin{bmatrix} A_R \sin(\omega t + \varphi) \\ \frac{A_I}{\omega} \cos(\omega t + \varphi) \end{bmatrix} = A_R \begin{bmatrix} \cos(\varphi) \\ \sin(\varphi) \end{bmatrix}, \quad (3)$$

$$T = \begin{bmatrix} \cos(\omega t) & \sin(\omega t) \\ -\sin(\omega t) & \cos(\omega t) \end{bmatrix}$$

Applying KVL to the AC side of the PV system in Fig. 1 results in the following equation:

$$-e_{inv} + L_S \frac{di}{dt} + R_S i + v_{Grid} = 0 \quad (4)$$

here, v_{Grid} is the AC grid voltage at PCC and e_{inv} represents the produced voltage of the multilevel inverter. Transforming this equation to dq coordinates by (3) leads to the following equations:

$$\begin{cases} \frac{d}{dt} I_d = -\frac{R_S}{L_S} I_d + \omega I_q + \frac{1}{L_S} E_{inv,d} - \frac{1}{L_S} V_{Grid,d} \\ \frac{d}{dt} I_q = -\frac{R_S}{L_S} I_q - \omega I_d + \frac{1}{L_S} E_{inv,q} - \frac{1}{L_S} V_{Grid,q} \end{cases} \quad (5)$$

where, $E_{inv,d}$ and $E_{inv,q}$ are d - and q -axis components of

multilevel inverter's voltage, respectively, $V_{Grid,d}$ and $V_{Grid,q}$ represent d - and q -axis components of AC grid voltage, and correspondingly, I_d and I_q are d - and q -axis current components. In the dq rotary frame, active and reactive power in the AC side of the PV system can be defined by the following equations:

$$\begin{cases} P = \frac{1}{2} (V_{Grid,d} I_d + V_{Grid,q} I_q) \\ Q = \frac{1}{2} (V_{Grid,d} I_q - V_{Grid,q} I_d) \end{cases} \xrightarrow[V_{Grid,q}=0]{V_{Grid,d}=|V|} \begin{cases} I_d = \frac{2P}{|V|} \\ I_q = \frac{2Q}{|V|} \end{cases} \quad (6)$$

Aligning d -axis of dq rotary frame to $V_{Grid,d}$ results in $V_{Grid,q} = 0$ and $V_{Grid,d} = |V|$ in which $|V|$ is the amplitude of AC grid voltage. As a result, (6) shows that the active and reactive powers can be independently controlled by d - and q -axis currents, respectively. Fig. 4 presents the block diagram of the modified decoupled current controller at the basis of derived equations in dq coordinates. It can be seen that the reference of active power, specified by a PI controller, is dedicated to the regulation of the summation of DC voltages. Also, the reactive power reference (Q_{ref}) is commanded by a higher control level having an appropriate power factor correction.

5 Proposed Two-Step Switching Technique

After calculation of reference voltages in dq coordinates ($V_{ref,d}$ and $V_{ref,q}$) by the modified decoupled current controller, these values are given to the two-step hybrid switching technique, as Fig. 5 shows. In this section, two parallel steps of the proposed technique, which are overviewed in section 3, are described in detail.

5.1 Step 1: Fast MPPT by SPWM Switching Technique

In steady-state conditions, the PV system is governed by a fundamental frequency-based switching technique.

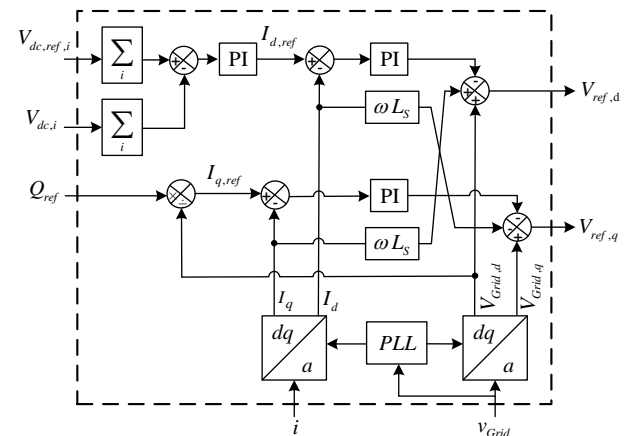


Fig. 4 The block diagram of the modified decoupled current controller.

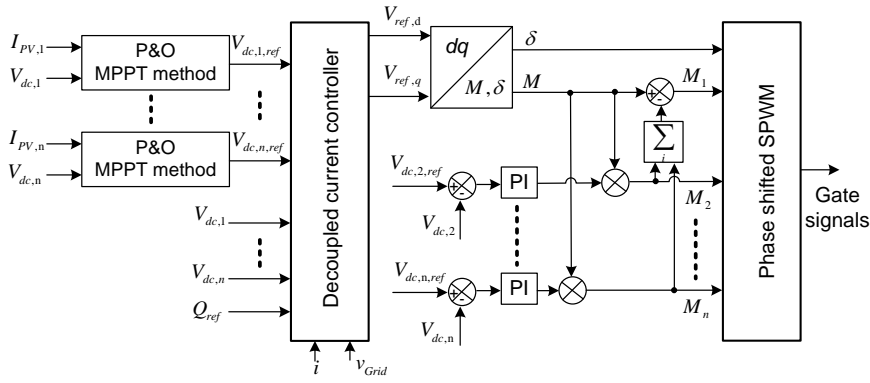


Fig. 5 Block diagram of step 1.

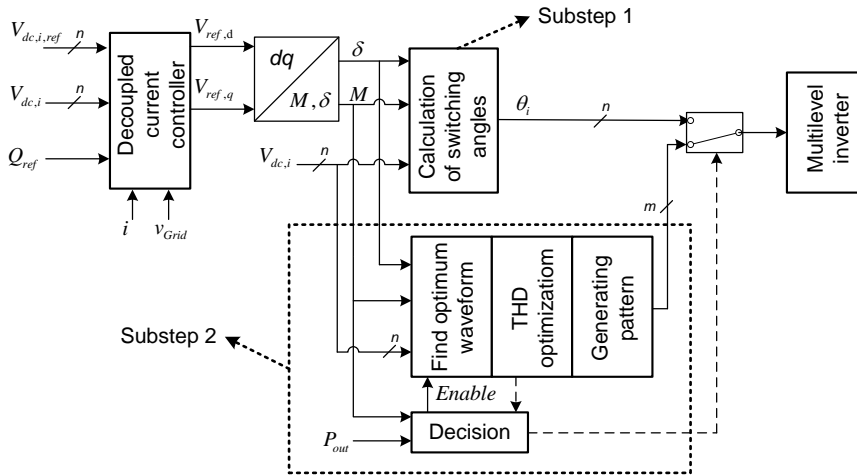


Fig. 6 Block diagram of two parallel substeps of step 2.

Upon a change in ambient conditions such as total or partial shading, step 1 with the presented block diagram in Fig. 5 activates to find new MPP of each PV module. Since the utilized SPWM switching technique increases the power losses, inappropriate activation of this step should be avoided. Therefore, those active power changes higher than ε_p , as the sign of happening a variation in ambient conditions, only can activate step 1 (see Fig. 3).

The presented block diagram of step 1 in Fig. 5, inspired by [21], shows that the MPP of each PV module is separately found by the standard P&O method. Also, it is seen that MPPT control signals as well as commanded reactive power are given to the modified decoupled current controller for generating d - and q -axis voltage references. Considering (7) clears that these two reference values are utilized to synthesize the modulation index (M) and the voltage phase angle (δ) for active and reactive power control.

$$M = \frac{\sqrt{(V_{ref,d})^2 + (V_{ref,q})^2}}{\sum_{i=1}^n V_{dc,i}}, \quad \delta = \text{tg}^{-1} \left(\frac{V_{ref,q}}{V_{ref,d}} \right) \quad (7)$$

Afterward, the obtained modulation index (M) is

employed besides the PI controller of i -th DC voltage to produce modulation index of i -th stage of cascaded multilevel inverter (M_i) for $i = 2, \dots, n$. However, the first modulation index (M_1) is obtained by (8), since the summation of M_i for $i = 1, \dots, n$ should be equal to the calculated M in (7).

$$M_1 = M - \sum_{i=2}^n M_i \quad (8)$$

5.2 Step 2: Power Losses Reduction and THD Minimization

At the end of step 1, all PV modules, regardless of experiencing partial shading conditions, operate in their MPPs, so the fundamental frequency-based technique can be utilized again to reduce power losses and minimize THD. As it is specified in Figs 3 and 6, two parallel substeps begin with activation of step 2, so the detailed explanation of these substeps is presented in the following.

5.2.1 Substep 1: DC Voltage Regulation

As it was mentioned, the modified decoupled current controller could not independently regulate each PV

module at its optimal voltage. Therefore, a supplementary control system, inspired by [22, 23], is proposed to independent regulation of DC voltages. At first, the Fourier analysis of produced voltage by a cascaded multilevel inverter with n unequal DC sources is considered:

$$V_o(t) = \sum_{k=1}^{\infty} V_k \sin(k\omega t),$$

$$V_k = \begin{cases} \frac{4}{k\pi} (V_{dc,1} \cdot \cos(k\theta_1) + \dots + V_{dc,n} \cdot \cos(k\theta_n)), & \text{odd } k \\ 0 & \text{even } k \end{cases} \quad (9)$$

where, V_k represents the amplitude of k -th voltage harmonic, $V_{dc,i}$ and θ_i for $i = 1, \dots, n$ are the voltage of i -th unequal DC source and switching angle, respectively. By considering the fundamental component of this waveform, modulation index (M) can be defined by (10), as the normalized value of the fundamental component:

$$M = \frac{V_1}{\sum_{i=1}^n V_{dc,i}} = \frac{\frac{4}{\pi} (V_{dc,1} \cdot \cos(\theta_1) + \dots + V_{dc,n} \cdot \cos(\theta_n))}{\sum_{i=1}^n V_{dc,i}} \quad (10)$$

As it has been introduced in [22], the voltage of each DC capacitor in the cascaded multilevel inverter can be regulated by its charging control. In the PV system, the generated power of each PV module is injected to its relevant DC capacitor and then delivered to the AC system, after subtraction of conduction as well as switching losses. Therefore, the voltage of each DC capacitor can be easily regulated by controlling its delivered power. Since a fundamental frequency-based switching technique is employed and DC voltages should be fixed at their optimal values, charge control can be obtained through switching angles.

With the assumption of a harmonic-free current in AC side of the multilevel inverter due to an appropriate harmonic filter, applying KCL at DC side of i -th H-bridge results in (11):

$$I_{c,i} = (I_{PV,i} - I_{loss,i}) - I_{inv} = I'_{PV,i} - I_{inv}$$

$$I_{inv} = I_m \sin(\omega t + \varphi), \quad I_{loss,i} = \frac{P_{loss,i}}{V_{dc,i}} \quad (11)$$

where, $I_{pv,i}$ is generated current of i -th PV module, $I_{c,i}$ and $P_{loss,i}$ are representative of capacitor current and power losses of i -th H-bridge, respectively. Moreover, the phase angle between the grid voltage and current is shown by φ and I_m is the amplitude of the AC side current of multilevel inverter (I_{inv}). To obtain equivalent losses current ($I_{loss,i}$), the calculated power losses of each H-bridge is divided by its relevant DC voltage. Since the power loss of each H-bridge is supplied by its connected PV module, the net injected current is

specified by $I'_{pv,i}$. It is worth mentioning that the introduced method in [24] is employed in the present study to calculate conduction and switching power losses. In this method, power losses are calculated at the basis of datasheet values and/or experimental measurements with minimum effort, high accuracy and little impact on the simulation time.

The average charge of i -th DC capacitor can be obtained by:

$$\bar{Q}_i = \frac{1}{T} \int_0^T [I'_{PV,i} - I_m \sin(\omega t + \varphi)] dt \quad (12)$$

Due to the operation of i -th H-bridge, I_{inv} flows into its DC and AC sides for $[\theta_i, \pi - \theta_i]$ and $[\pi + \theta_i, 2\pi - \theta_i]$, respectively. For other intervals of the switching cycle, short-circuiting of AC side results in isolation of DC capacitor from this side. Therefore, (12) can be extended to (13):

$$\bar{Q}_i = \frac{1}{T} \int_0^T I'_{PV,i} dt - \frac{1}{2\pi} \left(\int_{\theta_i}^{\pi - \theta_i} (I_m \sin(\omega t + \varphi)) d\omega t + \int_{\pi + \theta_i}^{2\pi - \theta_i} (-I_m \sin(\omega t + \varphi)) d\omega t \right)$$

$$= I'_{PV,i} + \frac{2}{\pi} I_m \cos(\varphi) \cos(\theta_i) \quad (13)$$

Considering the effect of power losses as an independent branch in (11) leads to lossless H-bridges. Thus, power balance equation can be written for the single-phase cascaded multilevel inverter. In this balance equation, delivered active power to the AC grid (P_{out}) should be equal to the total extracted power of PV modules minus total power losses.

$$P_{out} = \frac{1}{2} V_1 I_m \cos \varphi = \sum_{j=1}^n (I_{PV,j} \times V_{dc,j} - I_{loss,j} \times V_{dc,j})$$

$$= \sum_{j=1}^n (I'_{PV,j} \times V_{dc,j}) \quad (14)$$

$$I_m \cos \varphi = \frac{\sum_{j=1}^n (I'_{PV,j} \times V_{dc,j})}{\frac{4}{\pi} \sum_{j=1}^n (V_{dc,j} \cos \theta_j)}$$

Substitution of (14) in (13) results in (15):

$$\bar{Q}_i = I'_{PV,i} + \frac{\sum_{j=1}^n (I'_{PV,j} \times V_{dc,j})}{2 \sum_{j=1}^n (V_{dc,j} \cos \theta_j)} \cos \theta_i \quad (15)$$

In steady state conditions, average charge of DC capacitors should be equal to zero having constant DC voltages:

$$\sum_{j=1}^n (2I'_{pv,i} \times \cos \theta_j + I'_{pv,j} \times \cos \theta_i) V_{dc,j} = 0, i = 1, \dots, n \quad (16)$$

Beside these charging equations, desired modulation index, defined by (10), should also be satisfied. Therefore, first equation of (16) is substituted by (10) to form a system of n -equation with n switching angles as their unknown variables. Solving this system of equations guarantees regulation of M as well as $V_{dc,i}$ for $i = 2, \dots, n$ at their desired values, and $V_{dc,1}$ can be easily controlled by regulation of DC voltages' summation through the modified decoupled current controller. It is worth mentioning that this system of equations can be simply turned to linear equations by considering $\cos(\theta_i)$ instead of θ_i for $i = 1, \dots, n$ as their variables.

Now, one may try to minimize the THD of obtained waveform with these switching angles. However, the given THD formula in (17) shows that no unspecified switching angles remains for employing in THD minimization procedure [25]. Indeed, THD value is completely specified by the present optimal DC voltages as well as reactive power reference.

5.2.1 Substep 2: THD minimization

The given THD formula in (17) has no degree of freedom for THD minimization, so substep 2 with the presented flowchart in Fig. 7 is proposed to minimize THD value. In this flowchart, optimal DC voltages ($V_{dc,i}$ for $i = 1, \dots, n$) are sorted from smallest to largest and then, their combinations $C(n, i)$ for $i = 1, \dots, n$ are obtained. Among achieved sets of DC voltages, the elements of those combinations with cardinality of at least 2 are separately summed. By sorting summation results as well as those combinations with cardinality of 1 from smallest to largest, a set of V'_i for $i = 1, \dots, k$ is obtained. This can produce a k -level waveform with k switching angles, as shown in Fig. 8. Since DC voltages as well as reactive power can be regulated by n switching angles, $k-n$ switching angles remain that can be utilized as degrees of freedom for THD minimization.

It is worth mentioning that the equality of some DC

voltages decreases the number of obtainable voltage levels. Accordingly, Equality of all DC voltages, as the worst case, results in a waveform without the capability of THD minimization.

Now, similar to substep 1, the average charge of each DC capacitor should be set to zero. Considering Table 1, which specifies the number of repetitions for each DC voltage in different combination sets, may help to write charging equations. It is assumed that the assigned numbers to DC voltages indicate their rank, so $V_{dc,1}$ and $V_{dc,n}$ have the smallest and largest values, respectively.

Regarding the number of repetitions for i -th DC voltage in different combination sets, the charging equation of i -th DC capacitor can be obtained by (18).

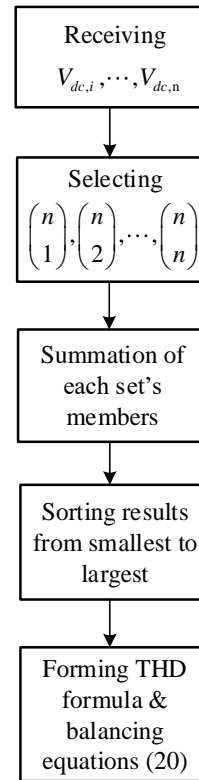


Fig. 7 Flowchart of substep 2.

$$THD = \sqrt{\frac{\pi}{4} \left[\frac{V_{dc,1}^2 (\theta_2 - \theta_1) + (V_{dc,1} + V_{dc,2})^2 (\theta_3 - \theta_2) + \dots + (V_{dc,1} + \dots + V_{dc,n-1})^2 (\theta_n - \theta_{n-1}) + (V_{dc,1} + \dots + V_{dc,n})^2 \left(\frac{\pi}{2} - \theta_n\right)}{(V_{dc,1} \cdot \cos(\theta_1) + V_{dc,2} \cdot \cos(\theta_2) + \dots + V_{dc,n} \cdot \cos(\theta_n))^2} \right] - 1} \quad (17)$$

$$\begin{aligned} \bar{Q}_i &= \frac{1}{T} \int_0^T I'_{pv,i} dt \\ &= -\frac{1}{2\pi} \sum_{p=1}^{r-1} \left[\int_{\theta_p}^{\theta_{p+1}} (I_m \sin(\omega t + \varphi)) d\omega t + \int_{\pi-\theta_{p+1}}^{\pi-\theta_p} (I_m \sin(\omega t + \varphi)) d\omega t + \int_{\pi+\theta_p}^{\pi+\theta_{p+1}} (-I_m \sin(\omega t + \varphi)) d\omega t + \int_{2\pi-\theta_{p+1}}^{2\pi-\theta_p} (-I_m \sin(\omega t + \varphi)) d\omega t \right] \\ &= -\frac{1}{2\pi} \left[\int_{\theta_k}^{\frac{\pi}{2}} (I_m \sin(\omega t + \varphi)) d\omega t + \int_{\frac{\pi}{2}}^{\pi-\theta_k} (I_m \sin(\omega t + \varphi)) d\omega t + \int_{\pi+\theta_k}^{\frac{3\pi}{2}} (-I_m \sin(\omega t + \varphi)) d\omega t + \int_{\frac{3\pi}{2}}^{2\pi-\theta_k} (-I_m \sin(\omega t + \varphi)) d\omega t \right] \\ &= I'_{pv,i} - \frac{2}{\pi} I_m \cos(\varphi) \left[\sum_{p=1}^{r-1} (\cos(\theta_p) - \cos(\theta_{p+1})) + \cos(\theta_k) \right] \end{aligned} \quad (18)$$

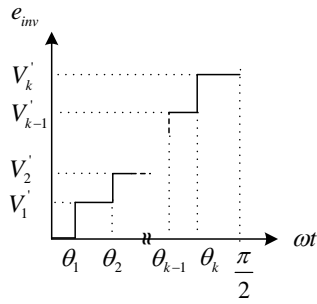


Fig. 8 The produced staircase waveform in substep 2.

Table 1 Repetitions of each DC voltage in the obtained combination sets.

Number of voltage levels & switching angles	The value of voltage levels	Number of repetitions for each DC voltage
$\binom{n}{1}$	$V_{dc,1}, \dots, V_{dc,n}$	1
$\binom{n}{2}$	$(V_{dc,1}+V_{dc,2}), \dots, (V_{dc,n-1}+V_{dc,n})$	$n-1$
$\binom{n}{3}$	$(V_{dc,1}+V_{dc,2}+V_{dc,3}), \dots, (V_{dc,n-2}+V_{dc,n-1}+V_{dc,n})$	$\frac{(n-1)(n-2)}{2}$
\vdots	\vdots	\vdots
$\binom{n}{n}$	$V_{dc,1}+\dots+V_{dc,n}$	1

where, θ_k is the last and bigger switching angle and r indicates the repetitions of each DC voltage. Similar to (14), applying active power balance between AC and DC sides of PV system results in (19)

$$\overline{Q}_i = I'_{PV,i} - \frac{\sum_{j=1}^n (I'_{PV,j} \times V_{dc,j})}{2 \sum_{j=1}^n (V_{dc,j} \cos \theta_j)} \times \left(\sum_{p=1}^{r-1} [\cos(\theta_p) - \cos(\theta_{p+1})] + \cos(\theta_k) \right) \quad (19)$$

$$THD = \sqrt{\frac{\pi}{4} \left(\frac{(V_1')^2 (\theta_2 - \theta_1) + (V_2')^2 (\theta_3 - \theta_2) + \dots + (V_{k-1}')^2 (\theta_k - \theta_{k-1}) + (V_k')^2 \left(\frac{\pi}{2} - \theta_k \right)}{(V_1' \cdot \cos(\theta_1) + (V_2' - V_1') \cos(\theta_2) + \dots + (V_k' - V_{k-1}') \cdot \cos(\theta_k))^2} \right)} - 1 \quad (21)$$

Setting these charging equations to zero in steady state conditions form a system of n -equation with k switching angles as their unknown variables in (20):

$$\sum_{j=1}^n \left(2I'_{PV,i} \times \cos \theta_j - I'_{PV,j} \times \cos \theta_i \right) \times \left(\sum_{p=1}^{r-1} [\cos(\theta_p) - \cos(\theta_{p+1})] + \cos(\theta_k) \right) V_{dc,j} = 0 \quad \text{for } i=1, \dots, n \quad (20)$$

Due to higher number of variables in comparison with equations, no unique solution set can be found for (20). However, these extra switching angles give the opportunity of performing THD minimization procedure, in contrast with substep 1. Therefore, an optimization problem with given THD formula in (21) as its objective function is formed.

The equality constraints of this problem consist of charging equations in (20) for $i = 2, \dots, n$ as well as defined modulation index in (10). It is worth mentioning that charge equation for $i = 1$ in (20) can also be considered along with other equality constraints when enough switching angles are available for THD minimization.

6 Simulation Results

In this section, the validity of proposed hybrid technique is confirmed by the simulation of a test PV system with both proposed and conventional SPWM [21] switching techniques in MATLAB/Simulink under various partial shading conditions. It should be remembered that the conventional SPWM is employed in step 1 of the proposed switching technique. Moreover, considering given parameters in Table 2 shows that the test PV system with AC-module architecture needs more than three sets of H-bridge & PV module to meet grid voltage level. Since increasing the number of these sets results in many figures, it is assumed that a string of three series PV modules is connected to each H-bridge.

Table 2 The parameters of PV test system.

Grid	Voltage	220 V, 50 Hz	
Each PV module at STC (Trina Solar TSM-250PA05.08) [26]	Open circuit voltage	37.6 V	
	Short circuit current	8.55 A	
	Nominal power	249.86 W	
	Number of H-bridges (stages)	3	
Cascaded multilevel inverter	IGBT Module (MG1215H-XBN2MM) [27]	1200 V, 15 A	
	Thermal resistance	Case to sink	0.02 K/W
		Sink to ambient	0.072 K/W
	DC capacitor	C_i	3 mF
	Switching frequency (SPWM technique)	f_{sw}	16 kHz
	Harmonic filter		16 mΩ, 4 mH

6.1 Simplifying Formulas

In the previous section, general formulas to calculate appropriate switching angles in the both substeps of step 2 are derived. Now, these formulas are simplified for the test PV system, which includes a three-stage single-phase multilevel inverter. In the substep 1, three optimal DC voltages, specified in step 1, produce a 7-level waveform with three switching angles. Considering charging equations of DC capacitors No. 2 and 3 as well as the modulation index formula result in a system of three equations with three unknown switching angles in (22).

All switching angles are completely specified by solving this system of equations, so presented THD formula in (23) results in a definite value without the possibility of THD minimization. If a partial shading condition leads to three different optimal DC voltages, performing substep 2 leads to a 15-level waveform with seven switching angles. Since there are small differences between the derived formulas for two parallel substeps of the step 2, simplified formulas of substep 2 are not mentioned here.

6.1 Partial Shading Condition

At the beginning, all PV modules receive uniform solar radiation (1000W/m^2) and operate in same ambient temperature (25°C) (see Fig. 9). Moreover, it is assumed that three PV modules of each string, which is connected to one H-bridge of the three-stage multilevel inverter, experience same conditions. In the presented figures of this section, each string is nominated by PV_i for $i = 1, 2, 3$.

Due to receiving similar solar radiation by all PV strings before $t = 0.1\text{sec.}$, operation of modules in same optimal DC voltages can be seen in Fig. 10. Moreover, a voltage ripple can be distinguished in the conventional technique as a result of continuous operation of the standard P&O method. These ripples can be compared with the smooth voltages of the proposed switching technique in which unnecessary operation of MPPT system is prevented. Fig. 11 shows that these voltage ripples affect the harvested power of PV modules.

Since three DC voltages are equal before $t = 0.1\text{sec.}$, the three switching angles of produced 7-level

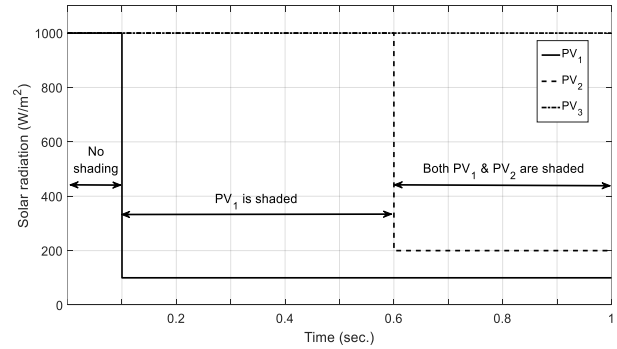


Fig. 9 Received solar radiation of PV_1 to PV_3 in the partial shading conditions.

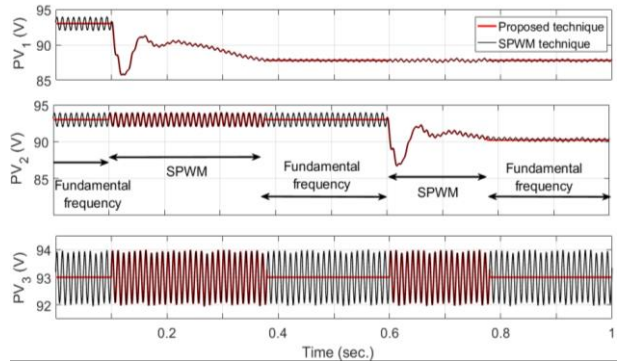


Fig. 10 Terminal voltage of PV strings.

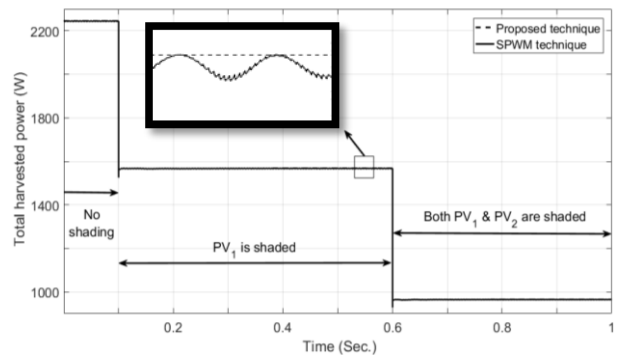


Fig. 11 Total harvested power with conventional and proposed switching techniques.

$$\begin{cases} \frac{4}{\pi}(V_{dc,1} \cdot \cos \theta_1 + V_{dc,2} \cdot \cos \theta_2 + V_{dc,3} \cdot \cos \theta_3) = M \times (V_{dc,1} + V_{dc,2} + V_{dc,3}) \\ (2I'_{PV,2} \times V_{dc,1}) \cos \theta_1 + (I'_{PV,1} \times V_{dc,1} + 3I'_{PV,2} \times V_{dc,2} + I'_{PV,3} \times V_{dc,3}) \cos \theta_2 + (2I'_{PV,2} \times V_{dc,3}) \cos \theta_3 = 0 \\ (2I'_{PV,3} \times V_{dc,1}) \cos \theta_1 + (2I'_{PV,3} \times V_{dc,2}) \cos \theta_2 + (I'_{PV,1} \times V_{dc,1} + I'_{PV,2} \times V_{dc,2} + 3I'_{PV,3} \times V_{dc,3}) \cos \theta_3 = 0 \end{cases} \quad (22)$$

$$THD = \sqrt{\frac{\pi}{4} \left(\frac{V_{dc,1}^2 (\theta_2 - \theta_1) + (V_{dc,1} + V_{dc,2})^2 (\theta_3 - \theta_2) + (V_{dc,1} + V_{dc,2} + V_{dc,3})^2 \left(\frac{\pi}{2} - \theta_3\right)}{(V_{dc,1} \cdot \cos(\theta_1) + V_{dc,2} \cdot \cos(\theta_2) + V_{dc,3} \cdot \cos(\theta_3))^2} \right) - 1} \quad (23)$$

waveform cannot be increased by the proposed method in substep 2. However, the presented THD value in Fig. 12 is still smaller than that of the conventional SPWM. In addition, Fig. 13 clears that the proposed hybrid switching technique can expectedly reduce power losses in comparison with conventional SPWM. It is worth mentioning that the presented curves in the datasheet of the utilized IGBT module are employed for calculation of conduction as well as switching losses.

At $t = 0.1\text{sec.}$, PV_1 experiences an exaggerative transient shadow, which decreases its received solar radiation to 100W/m^2 . The consequent reduction of harvested power activates step 1 of the proposed switching technique finding optimal DC voltages for PV_1 to PV_3 . Fig. 10 shows that the optimal voltage of partially shaded PV_1 is found during 0.2 seconds, while no new optimal voltages are found for PV_2 and PV_3 . Since step 1 employs the SPWM technique, both conventional SPWM and proposed switching techniques result in similar voltage ripples. In addition, increasing THD value as well as power losses can be seen in Figs. 12 and 13, respectively.

It is worth mentioning that steadily decrement of power losses during this interval, which occurs for both techniques, is due to the reduction of total harvested power in the present partial shading condition. Moreover, due to temperature dependence of power losses as well as large time-constant of heat transfer systems, slow dynamic response can be seen for both techniques in

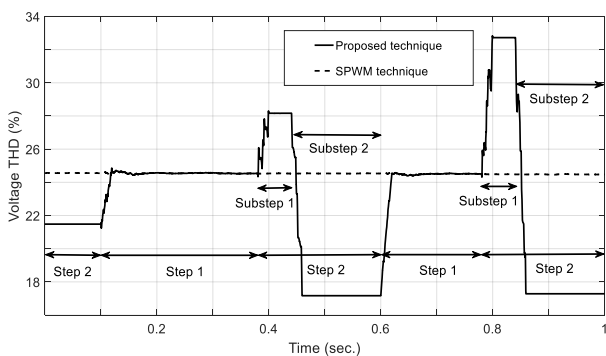


Fig. 12 THD of produced voltage with conventional and proposed switching techniques.

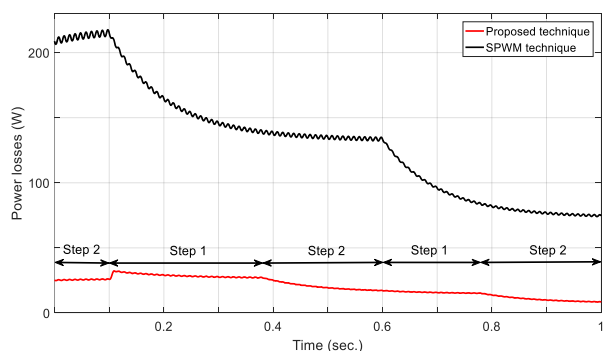
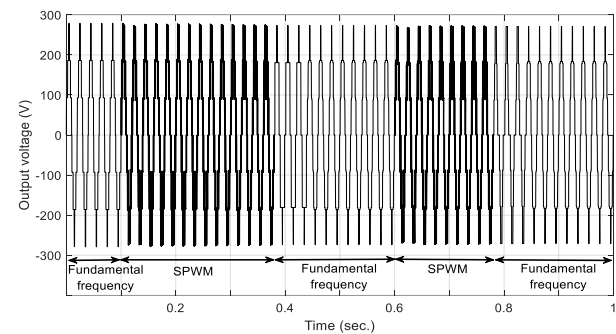


Fig. 13 Total power losses of the test PV system with conventional and proposed switching techniques.

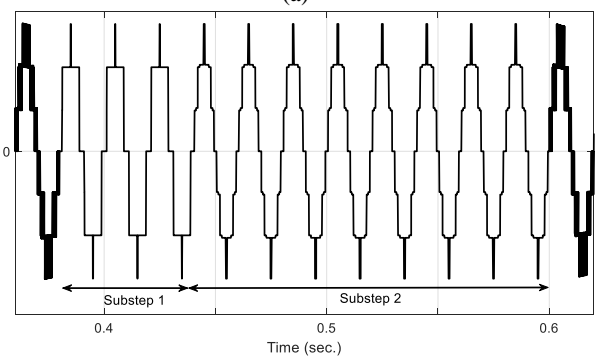
In addition, different initial junction temperatures can describe the reason for the large difference in power losses between conventional and proposed methods during step 1, when both switching techniques employ conventional SPWM. Besides, Figs 10 and 12 show that the step 1 lasts only for short-time intervals, so the junction temperature in the proposed switching technique cannot reach to those higher temperatures in the conventional SPWM.

Upon finding optimal voltages, appropriate switching angles to regulate DC voltages, as well as modulation index, are immediately calculated by substep 1. In consequence, Fig. 14 shows that the utilized switching technique is changed from SPWM to the fundamental frequency-based technique. Besides, substep 2 is also in progress to obtain a waveform with higher number of switching angles and lower THD value. Fig. 14 shows that after a few cycles, the optimization procedure finishes and as a result, an eleven-level voltage with five switching angles is obtained for the steady-state condition. Fig. 12 reveals that the THD value of the produced voltage is significantly reduced. Comparing these results with those of conventional SPWM in Figs. 12 and 13 verify the superiority of the proposed hybrid switching technique.

At $t = 0.6\text{sec.}$, PV_2 experiences a partial shading, and its received solar radiation is decreased to 200W/m^2 . The consequent change in the extracted power activates step 1 of the proposed switching technique and Fig. 10 shows that optimal DC voltages are quickly found at $t = 0.7\text{sec.}$, similar to the conventional SPWM. Upon finding optimal DC voltages and activation of the



(a)



(b)

Fig. 14 Produced voltage by the proposed switching technique besides its zoomed figure.

Table 3 The simulation results of both switching techniques under various partial shading conditions.

Partially shaded PV strings	Conventional SPWM technique		The proposed hybrid switching technique					
	THD [%]	Steady-state power losses [W]	Number of different optimal DC voltages	Step 1		Step 2		Steady-state power losses [W]
				Number of levels & switching angles	THD [%]	Number of levels & switching angles	THD [%]	
No string	24.5	216	1	7 levels 3 angles	21.48	7 levels 3 angles	21.48	26
PV ₁		133.5	2	7 levels 3 angles	28.17	11 levels 5 angles	17.17	16
PV ₁ & PV ₂		73.5	3	7 levels 3 angles	32.74	15 levels 7 angles	17.27	8

step 2, the utilized switching technique is returned to the fundamental frequency-based technique and consequently, a 7-level output waveform is produced. By finalizing optimization procedure in substep 2 and estimation of optimal switching angles, Figs. 12 and 14 reveal that a 15-level waveform with THD = 17.27% is produced. Comparing with the previous partial shading condition, three different optimal DC voltages are obtained here. Therefore, a waveform with higher number of levels and lower THD value has been achieved. Moreover, Fig. 13 presents lower power losses for both techniques, since the total harvested power is reduced in this new condition. Besides, it is seen that the response of conventional technique against this new-happened partial shading is similar to the previous condition, which occurred at $t = 0.1$ sec.

For the sake of comparison, the obtained results of both proposed and conventional switching techniques under mentioned partial shading conditions are summarized in Table 3. This table presents the outstanding ability of the proposed hybrid switching technique to reduce the power losses and consequently, increase the solar energy conversion efficiency. Moreover, it is seen that the THD minimization ability of the proposed switching technique is increased by the intensity of partial shading conditions. However, there is no control over the THD value when all PV modules experience the same ambient conditions and operate in similar optimal DC voltages.

It should be noted that the THD value for conventional SPWM changes in accordance with variation of optimal voltage of PV modules. However, small changes in PV modules' optimal voltages lead to a trivial variation of THD value in Fig. 12, so a fixed THD amount is brought in Table 3 for the conventional SPWM.

7 Conclusion

In this paper, a hybrid switching technique is introduced for a single-phase domestic PV system with AC-module architecture. In this PV system, PV modules are directly connected to DC terminals of a cascaded multilevel inverter without any DC optimizer because of the ability of the proposed switching technique for independent regulation of DC voltages. As

one of the main contributions of the proposed hybrid technique, power losses are reduced by employing a fundamental frequency-based switching technique to increase the efficiency of the solar energy conversion system. In addition, the fast dynamic response of the PV system with the proposed hybrid technique is observed due to the appropriate combination of SPWM and fundamental frequency switching techniques. This leads to harvest more power in partial shading conditions. THD minimization is another advantage of the proposed switching technique that is obtained by introducing a novel method to produce a waveform with higher number of levels. These advantages are verified by simulation of a test PV system in MATLAB/Simulink with both conventional SPWM and proposed switching techniques under various partial shading conditions.

References

- [1] J. L. Acosta, K. Combe, S. Ž. Djokic, and I. Hernando-Gil, "Performance assessment of micro and small-scale wind turbines in urban areas," *IEEE Systems Journal*, Vol. 6, No. 1, pp. 152–163, Mar. 2012.
- [2] K. G. Firouzjah, "Assessment of small-scale solar PV systems in Iran: regions priority potentials and financial feasibility," *Renewable and Sustainable Energy Reviews*, Vol. 94, pp. 267–274, Oct. 2018.
- [3] N. Karami, N. Moubayed, and R. Outbib, "General review and classification of different MPPT techniques," *Renewable and Sustainable Energy Reviews*, Vol. 68, pp. 1–18, Feb. 2017.
- [4] J. D. Bastidas-Rodriguez, E. Franco, G. Petrone, C. A. Ramos-Paja, and G. Spagnuolo, "Maximum power point tracking architectures for photovoltaic systems in mismatching conditions: a review," *IET Power Electronics*, Vol. 7, No. 6, pp. 1396–1413, Jun. 2014.
- [5] K. Lappalainen and S. Valkealahti, "Effects of irradiance transition characteristics on the mismatch losses of different electrical PV array configurations," *IET Renewable Power Generation*, Vol. 11, No. 2, pp. 248–254, Apr. 2017.

- [6] T. Ghanbari, "Permanent partial shading detection for protection of photovoltaic panels against hot spotting," *IET Renewable Power Generation*, Vol. 11, No. 1, pp. 123–131, Apr. 2017.
- [7] E. I. Batzelis, P. S. Georgilakis, and S. A. Papathanassiou, "Energy models for photovoltaic systems under partial shading conditions: a comprehensive review," *IET Renewable Power Generation*, Vol. 9, No. 4, pp. 340–349, Apr. 2015.
- [8] B. Liu, S. Duan, and T. Cai, "Photovoltaic DC-building-module-based BIPV system—concept and design considerations," *IEEE Transactions on Power Electronics*, Vol. 26, No. 5, pp. 1418–1429, May 2011.
- [9] N. Kumar, I. Hussain, B. Singh, and B. K. Panigrahi, "Rapid MPPT for uniformly and partial shaded PV system by using JayaDE algorithm in highly fluctuating atmospheric conditions," *IEEE Transactions on Industrial Informatics*, Vol. 13, No. 5, pp. 2406–2416, Oct. 2017.
- [10] A. Mohapatra, B. Nayak, P. Das, and K. B. Mohanty, "A review on MPPT techniques of PV system under partial shading condition," *Renewable and Sustainable Energy Reviews*, Vol. 80, pp. 854–867, Dec. 2017.
- [11] M. Amin, J. Bailey, C. Tapia, and V. Thodimeladine, "Comparison of PV array configuration efficiency under partial shading condition," in *IEEE 43rd Photovoltaic Specialists Conference*, pp. 3704–3707, 2016.
- [12] B. Xiao, L. Hang, J. Mei, C. Riley, L. M. Tolbert, and B. Ozpineci, "Modular cascaded H-bridge multilevel PV inverter with distributed MPPT for grid-connected applications," *IEEE Transactions on Industry Applications*, Vol. 51, No. 2, pp. 1722–1731, 2015.
- [13] D. Leuenberger and J. Biela, "PV-module-integrated AC inverters (AC modules) with subpanel MPP tracking," *IEEE Transactions on Power Electronics*, Vol. 32, No. 8, pp. 6105–6118, Aug. 2017.
- [14] W. Xiao, M. S. El Moursi, O. Khan, and D. Infield, "Review of grid-tied converter topologies used in photovoltaic systems," *IET Renewable Power Generation*, Vol. 10, No. 10, pp. 1543–1551, Nov. 2016.
- [15] A. Bidram, A. Davoudi, and R. S. Balog, "Control and circuit techniques to mitigate partial shading effects in photovoltaic arrays," *IEEE Journal of Photovoltaics*, Vol. 2, No. 4, pp. 532–546, Oct. 2012.
- [16] J. Kan, Y. Wu, Y. Tang, S. Xie, and L. Jiang, "Hybrid control scheme for photovoltaic microinverter with adaptive inductor," *IEEE Transactions on Power Electronics*, Vol. 34, No. 9, pp. 8762–8774, Sep. 2019.
- [17] K. Alluhaybi, I. Batarseh, H. Hu, and X. Chen, "Comprehensive review and comparison of single-phase grid-tied photovoltaic microinverters," *IEEE Journal of Emerging and Selected Topics in Power Electronics*, 2019.
- [18] M. Shiao and S. Moskowicz, "The global PV inverter landscape 2013: Technologies, markets and survivors," *GTM Research-Technical*, 2015.
- [19] N. Karami, N. Moubayed, and R. Outbib, "General review and classification of different MPPT Techniques," *Renewable and Sustainable Energy Reviews*, Vol. 68, pp. 1–18, Feb. 2017.
- [20] R. Zhang, M. Cardinal, P. Szczesny, and M. Dame, "A grid simulator with control of single-phase power converters in D-Q rotating frame," in *33rd Annual IEEE Power Electronics Specialists Conference*, 2002, pp. 1431–1436.
- [21] A. Roshan, R. Burgos, A. C. Baisden, F. Wang, and D. Boroyevich, "A d-q frame controller for a full-bridge single phase inverter used in small distributed power generation systems," in *22nd Annual IEEE Applied Power Electronics Conference and Exposition*, pp. 641–647, 2007.
- [22] Z. Liu, B. Liu, S. Duan, and Y. Kang, "A novel DC capacitor voltage balance control method for cascade multilevel STATCOM," *IEEE Transactions on Power Electronics*, Vol. 27, No. 1, pp. 14–27, Jan. 2012.
- [23] R. Sajadi, H. Iman-Eini, M. K. Bakhshizadeh, Y. Neyshabouri, and S. Farhangi, "Selective harmonic elimination technique with control of capacitive DC-link voltages in an asymmetric cascaded H-bridge inverter for STATCOM application," *IEEE Transactions on Industrial Electronics*, Vol. 65, No. 11, pp. 8788–8796, Nov. 2018.
- [24] U. Drogenik and J. W. Kolar, "A general scheme for calculating switching-and conduction-losses of power semiconductors in numerical circuit simulations of power electronic systems," in *International Power Electronic Conference*, Japan, 2005.
- [25] N. Farokhnia, S. H. Fathi, N. Yousefpoor, and M. K. Bakhshizadeh, "Minimisation of total harmonic distortion in a cascaded multilevel inverter by regulating voltages of dc sources," *IET Power Electronics*, Vol. 5, No. 1, pp. 106–114, Jan. 2012.

[26] Trina Solar,
<https://www.trinasolar.com/us/resources/downloads>,
accessed 20 Sep. 2019

[27] Power Module 1200V 15A IGBT Module,
“MG1215H-XBN2MM datasheet,” Littelfuse, 2016.



H. Toodeji was born in 1984 in Iran. He received B.Sc. in Electrical Engineering from Isfahan University of Technology, Isfahan, Iran in 2006. Also, he received both M.Sc. and Ph.D. degrees in Electrical Engineering from Amirkabir University of Technology (Tehran Polytechnic), Tehran, Iran, in 2009 and 2013, respectively. He is currently an

Assistant Professor at Yazd University, Yazd, Iran. His research interests include power electronics and renewable energy sources.



© 2020 by the authors. Licensee IUST, Tehran, Iran. This article is an open access article distributed under the terms and conditions of the Creative Commons Attribution-NonCommercial 4.0 International (CC BY-NC 4.0) license (<https://creativecommons.org/licenses/by-nc/4.0/>).